Progress In Electromagnetics Research C, Vol. 135, 43–53, 2023

Design of Compact Wide-Beam Broadband Antenna for Wide-Angle Scanning Applications

Da Yu, Hongmei Liu*, Shuo Li, Zhongbao Wang, and Shaojun Fang

Abstract—In this paper, a compact antenna with wideband and wide beam is proposed. It is composed of a rectangular patch etched on a substrate, a feeding probe, two metal columns, and a ground plane. By inserting air gap between the substrate and the ground, as well as using the coupled feeding, wide impedance bandwidth is obtained. By inserting two metal columns on the two sides of the patch for inducing longitudinal current, the HPBW of the antenna in the operation bandwidth can be widened. Design evolutions are provided for the proposed antenna, and main parameters are investigated for obtaining the adjusting rules. For validation, a prototype operating at 5.8 GHz is fabricated, where the dimension is only $0.31\lambda_0 \times 0.11\lambda_0 \times 0.11\lambda_0$. Measurement results show that a fractional bandwidth of 24% is achieved for $|S_{11}| < 10$ dB. In this bandwidth, the measured gain is larger than 2.5 dBi with a maximum gain of 3.5 dBi. At E-plane, the measured HPBWs are in the range of $130^\circ \sim 190^\circ$, and the values are around 120° at H-plane.

1. INTRODUCTION

With the rapid development of 5G technology, phased arrays have been widely used in military and civilian communications. The phase array with a wide scan angle can not only improve the detection range and accuracy of the radar but also enhance wireless connectivity for Internet of Things (IoT) applications. Adopting wide beamwidth and wideband antenna element is an effective method to support wide-angle and wideband scanning property, which has aroused the interest of many researchers in recent years [1, 2]. With the advantage of low cost and compactness, microstrip antennas are widely used in phased arrays. However, microstrip antenna exhibits a narrow bandwidth, and the typically half-power beamwidth (HPBW) is only 90°, which results in a limited scanning range of the antenna array [3]. In [4], a wide-beamwidth dual-polarized microstrip antenna fed by a differential network is proposed, which exhibits a 10-dB fractional bandwidth (FBW) of 9.9% and the HPBWs of around 115°. In [5], a simple and compact magnetic dipole is designed with the HPBWs of 150° and 130° in the E- and H-planes, respectively. However, the 10-dB FBW is only 2%. As an improvement, the multipole antenna which is composed by multiple magnetic and electric dipoles is proposed in [6], where the FBW is increased to 13%. In [7] and [8], metal walls are set on the bilateral sides of the patch antennas, which effectively improve the HPBWs, and the FBWs reach 15% and 17%, respectively. However, since the metal walls lead to high profile and heavy weight, the antenna is not convenient for application. Besides, the bandwidths for the above wide beam antennas are still not enough for 5G wideband applications. To further increase the bandwidth, an air cavity is embedded into the substrate of a patch antenna [9], which effectively extends the FBW to 40%. The HPBW is also increased to be more than 140°.

Except patch antenna, magnetoelectric (ME) dipole antennas are often combined for increasing the bandwidth [10, 11]. Thus, several methods are presented for improving the HPBW of magnetoelectric dipole antennas. In [12], the wide HPBW around 100° is obtained within 36.5% FBW by employing four L-shaped dipole arms and inclined sidewalls along the E-plane edge of the ground. In [13], by inserting

Received 24 April 2023, Accepted 21 June 2023, Scheduled 22 July 2023
* Corresponding author: Hongmei Liu (lhm323@dlmu.edu.cn).
The authors are with the School of Information Science and Technology, Dalian Maritime University, Dalian, Liaoning 116026, China.

two parasitic Π-shaped patches at the two sides of the ME dipole antenna, the HPBWs in both E- and H-planes are increased to be more than 120° over the bandwidth of 32.3%. In [14], a U-shaped reflector and a pair of L-shaped metal arms are served as the ME dipole to realize wideband and wide beam. In the bandwidth of more than 90%, the HPBW is within 100° ∼ 179° and 83° ∼ 146° in the H- and E-planes. To further increase the HPBW in wide bandwidth, metal columns are applied underneath the edge of the dipole [15, 16], where the HPBW can exceed 180°. Besides, a pair of parasitic patches with metallic vias arranged symmetrically on either side of the original electric dipoles is added in [17], resulting in almost omnidirectional radiation at the H-plane and about 156° HPBW at the E-plane. However, although the antennas in [14, 16, 17] are wideband antennas, only the HPBWs at the center frequency are provided, which is not enough to show the in-band wide beam performance. Except ME dipole antennas, some researches have been done on the HPBW enhancement of wideband dielectric resonator antenna (DRA) due to its advantages of high efficiency, low cost, and flexible structure. In [18], a metamaterial-based DRA fed with miniaturized equal-amplitude and out-of-phase Huygens sources is proposed, which exhibits an HPBW of 194° and an FBW of 14.1%. In [19], a grooved DRA with a comb-like metal wall is presented for operating in the bandwidth of 38.2%. In this bandwidth, the HPBWs are 120° ∼ 248° and 100° ∼ 150° in E- and H-planes, respectively. However, the expensive fabrications of DRAs limit large-scale applications

In this paper, a compact wideband antenna with wide beam is proposed. The bandwidth is broadened by inserting air gap, and the HPBWs are widened by two metal columns. For validation, a prototype operating at 5.8 GHz is fabricated, where the dimension is only $0.31\lambda_o \times 0.11\lambda_o \times 0.11\lambda_o$. Measurement results show that a fractional bandwidth of 24% is achieved for $|S_{11}| < 10$ dB. In this bandwidth, the measured gain is larger than 2.5 dBi with a maximum gain of 3.5 dBi. At E-plane, the measured HPBWs are in the range of 130° ∼ 190°, and the values are around 120° at H-plane. The organization of this paper is as follows. The antenna configuration and evolution are described in Section 2. Parametric studies are shown in Section 3. The performance of the antenna and the measured results are investigated in Section 4, followed by a conclusion in Section 5.

2. ANTENNA CONFIGURATION AND EVOLUTIONS

2.1. Antenna Configuration

Figure 1 shows the configuration of the proposed antenna, including the 3-D view, top view, and , side view. It consists of a radiation patch, an F4B substrate ($\varepsilon_r = 3.5$, $\tan\delta = 0.003$, $H_s = 1.5$ mm), a feeding probe, two metal columns, and a ground plane. The proposed antenna adopts a single coaxial feed at the bottom, where the outer conductor of the SMA connector is connected to the ground, and the inner conductor of the SMA connector is extended upward to align with the substrate. The radiation patch is on the top surface of the substrate ($L_s \times W_s$). The radiation patch is composed of a rectangular patch connected with a ring, where the width of the rectangular patch is W_1, and the diameter of the ring is R_P. The overall length of the radiation patch is L_1. Two circular slots with the diameters of R_{g1} and R_{g2}, respectively, are etched on the radiation patch for inserting the feeding probe and one metal column. The diameters of the feeding probe and metal column are denoted as R_f and R_1, respectively. The distance between the feed point and the substrate left edge is L_g, and the distance between the center points of the feeding probe and the right metal column is L_2. The ground plane ($L_{gx} \times L_{gy}$) is made of copper sheets with a thickness of H_g. An air gap of H_a is inserted between the substrate and the ground plane for bandwidth enhancement.

2.2. Design Evolutions

For explaining the design process of the proposed antenna clearly, three steps depicting the evolution structure are shown in Fig. 2. Fig. 3 gives the equivalent circuits of each stage. For comparison, Figs. 4–6 give the simulated $|S_{11}|$, the radiation patterns at 5.8 GHz, and the in-band HPBWs of the three evolutions. The initial design starts from the traditional patch antenna. To obtain the original antenna parameters, the design formulas of the traditional patch antenna are used, as shown in (1).

$$L = \frac{\lambda_0}{2\sqrt{\varepsilon_e}} - 2\Delta l \tag{1a}$$

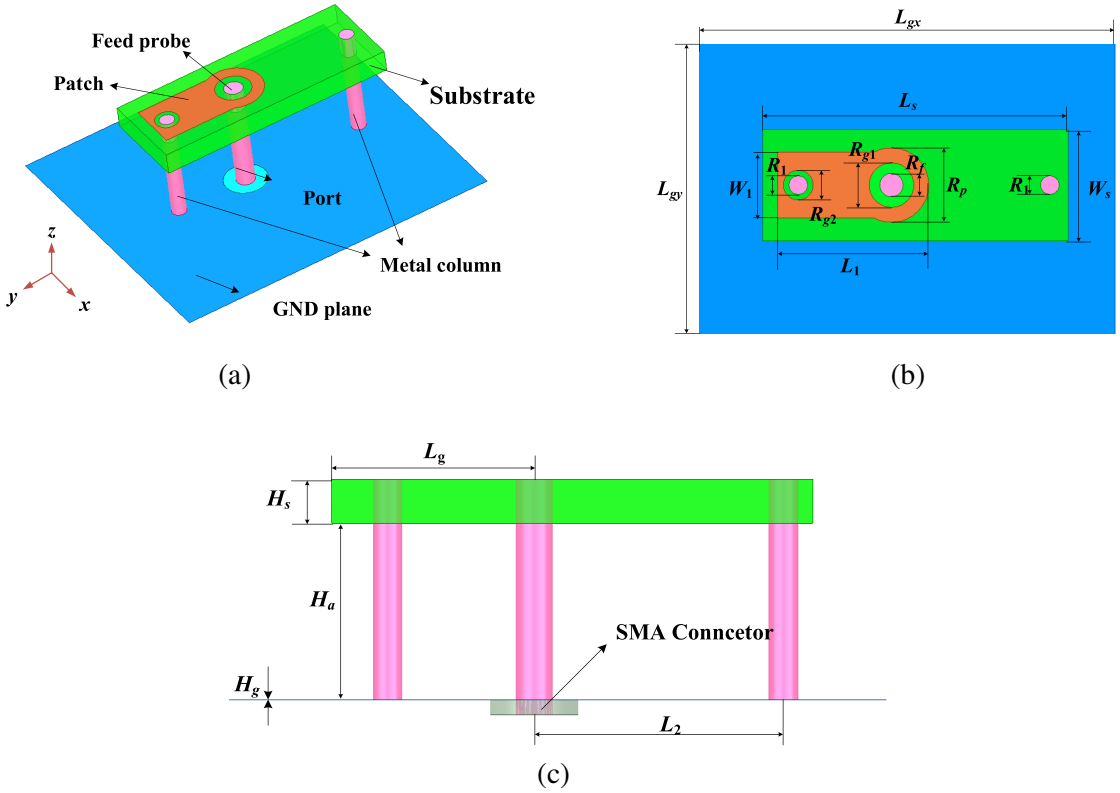

Figure 1. Configuration of the proposed antenna. (a) 3-D view. (b) Top view. (c) Side view.

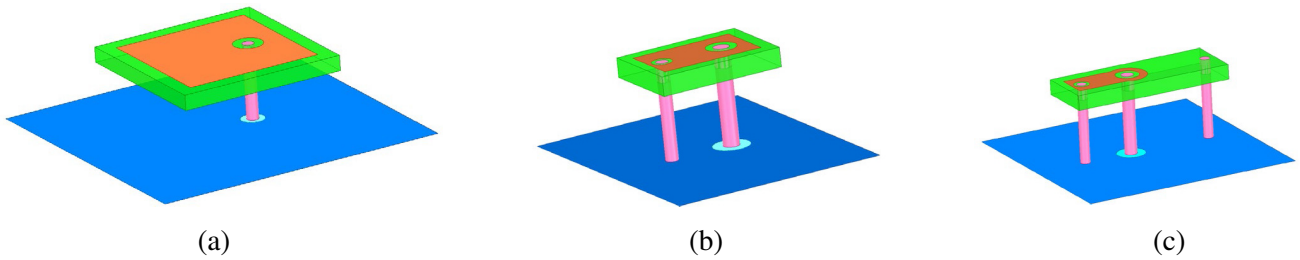

Figure 2. Evolutions of the proposed antenna. (a) Ant. 1. (b) Ant. 2. (c) Ant. 3.

$$\Delta l = 0.412H\frac{(\varepsilon_e + 0.3)\left(\frac{W}{H} + 0.264\right)}{(\varepsilon_e - 0.258)\left(\frac{W}{H} + 0.8\right)} \tag{1b}$$

Here, λ_0 is the wavelength at the center frequency; L and W are the length and width of the patch, respectively; and H is the thickness of the substrate. According to (1), the dimension of the traditional patch antenna is calculated as 14×14 mm. To widen the bandwidth, a modified patch antenna with coupled feeding is designed, named as Ant. 1. As can be seen in Fig. 4, wide 10-dB bandwidth of nearly 27.6% is obtained for Ant. 1 due to the neutralization of inductance and capacitance generated from the long probe and coupled feeding, respectively. Fig. 3(a) shows the equivalent circuit of Ant. 1. Here, variables L_2 and C_2 represent the equivalent resonant inductance and capacitance of the patch, respectively. Let L_1 be the equivalent inductor induced by the feeding probe and C_1 be the equivalent capacitor induced by the coupled feeding. R_1 and R_2 are the radiation resistors for the long feeding probe and the patch, respectively. With the parameters shown in Table 1, the input port impedance

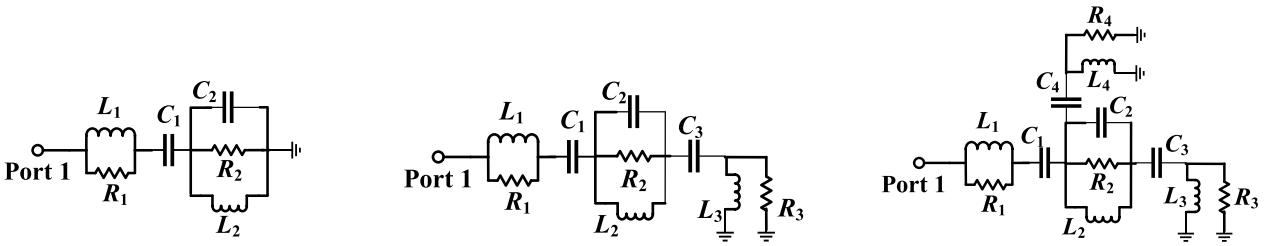

Figure 3. Equivalent circuit diagrams of the proposed antenna. (a) Ant. 1. (b) Ant. 2. (c) Ant. 3.

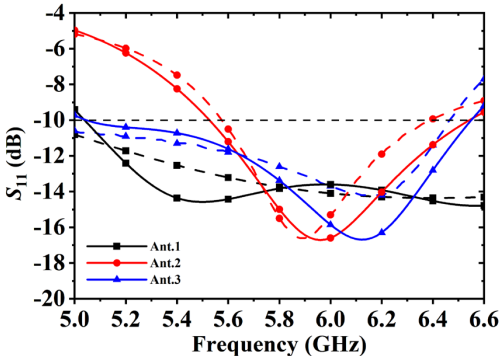

Figure 4. Simulated $|S_{11}|$ of the three evolutions in the model (line with symbol) and the equivalent circuit (dash line) versions.

Table 1. Parameters of the equivalent circuits for the three stages.

	R_1	R_2	R_3	R_4	C_1	C_2	C_3	C_4	L_1	L_2	L_3	L_4
Ant. 1	107 Ω	42 Ω	–	–	0.7 pF	20 pF	–	–	1.9 nH	1.6 nH	–	–
Ant. 2	70 Ω	30 Ω	70 Ω	–	5 pF	6.6 pF	11.9 pF	–	0.5 nH	0.12 nH	0.89 nH	–
Ant. 3	43 Ω	53 Ω	99 Ω	159 Ω	5 pF	6.6 pF	11.9 pF	0.13 pF	2 nH	0.15 nH	0.89 nH	4 nH

matching of the equivalent circuit in Fig. 3(a) can be obtained, as shown in Fig. 4 (red dash line). Fig. 5 shows the HPBWs at the E- and H-planes of 5.8 GHz. It is observed from Fig. 5 that the in-band HPBWs of Ant. 1 at E- and H-planes are in the range of $50^\circ \sim 70^\circ$ and $72^\circ \sim 80^\circ$, respectively.

To increase the HPBW, one metal column is inserted (named as Ant. 2), where one end is connected to the ground plane and the other coupled with the radiation patch. Since the long metal column will introduce a longitudinal current, the size of the antenna can be greatly reduced. In Ant. 1, the size of the substrate is 17 mm × 17 mm, and in Ant. 2, it is reduced to 7 mm × 10 mm (the distance between the edges of the patch and substrate is fixed.) Fig. 3(b) gives the equivalent circuit of Ant. 2, where R_3 and L_3 denote the radiation resistor and equivalent inductor of the adding metal column, and C_3 represents the capacitance coupling for the metal column. Good consistency for the impedance matching is observed between the model and the equivalent circuit of Ant. 2, as shown in Fig. 4. Compared with Ant. 1, the 10-dB impedance bandwidth of Ant. 2 is narrowed to about 14.9%, but the HPBW can be increased. As can be seen in Fig. 5, the HPBW of Ant. 2 at the E-plane reaches 125°, while the HPBW at H-plane is slightly improved to 90°. As observed in Fig. 6, the in-band HPBWs of Ant. 2 at E- and H-planes are in the range of 110° to 150° and 90° to 98°, respectively. However, one problem is that the maximum radiation direction at the E-plane shifts to 60°. This may be due to the strong radiation of the long feeding probe compared with the left metal column. To correct the beam pointing at E-plane, another metal column is inserted (named as Ant. 3), where one end is connected to the ground plane,

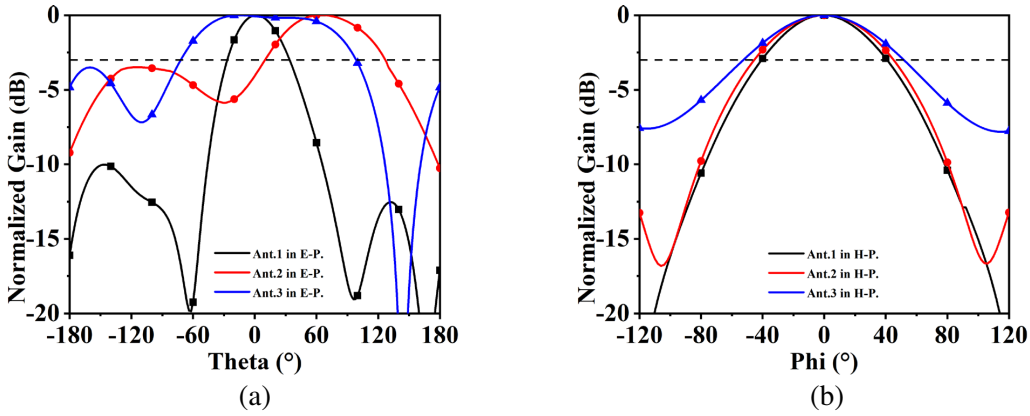

Figure 5. Simulated radiation patterns of the three evolutions at 5.8 GHz. (a) E-plane. (b) H-plane.

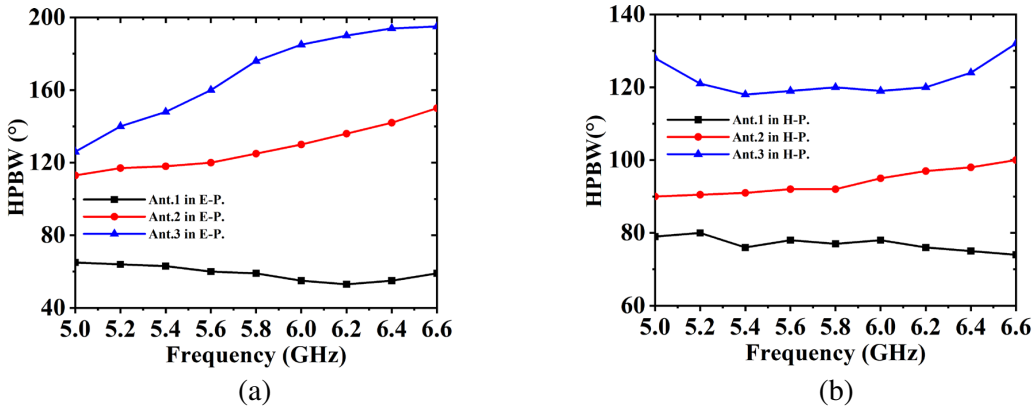

Figure 6. Simulated in-band HPBWs of the three evolutions. (a) E-plane. (b) H-plane.

and the other is connected to the substrate. Since the right metal column introduces an opposite current compared with the feeding probe, the radiation of the right side is decreased, and the radiation of the left side is increased. After optimization, the size of the substrate for Ant. 3 is 5 mm × 16 mm which is reduced by 40% compared to Ant. 1. Fig. 3(c) shows the equivalent circuit of Ant. 3, where R_4 and L_4 denote the radiation resistor and equivalent inductor of the second metal column, and C_4 represents the capacitance coupling for the metal column. According to the parameters in Table 1, the result of the equivalent circuit agrees well with the layout model. As seen in Fig. 5, the maximum radiation at the E-plane can be adjusted to the main direction, and the radiation pattern becomes symmetrical. Besides, at 5.8 GHz, the HPBWs at E-plane and H-plane are 170° and 120°, respectively. As seen in Fig. 6, the insertion of the right metal column effectively increases the in-band HPBW at both E- and H-planes, while the HPBW at the H-plane trends more stable. From 5 GHz to 6.5 GHz, the in-band HPBWs of Ant. 3 are in the ranges of 121° ∼ 190° and 118° ∼ 129° at E- and H-planes, respectively.

3. PARAMETRIC STUDIES

In this section, the influences of several representative parameters are studied. Results are obtained with the simulator Ansoft HFSS. Here, the performances of impedance matching (S_{11}), gain, and HPBW are investigated. Four variations are chosen, including the dimension of the radiation patch (W_1 and L_1), the distance of the right metal column from the feeding probe (L_2), the height of metal columns (H_a), and the width of the ground (L_{gy}). It is noted that when one parameter is investigated, the others are maintained as the optimized values.

Figure 7 shows the performances of the proposed antenna with different W_1 ranging from 2 to 4 mm.

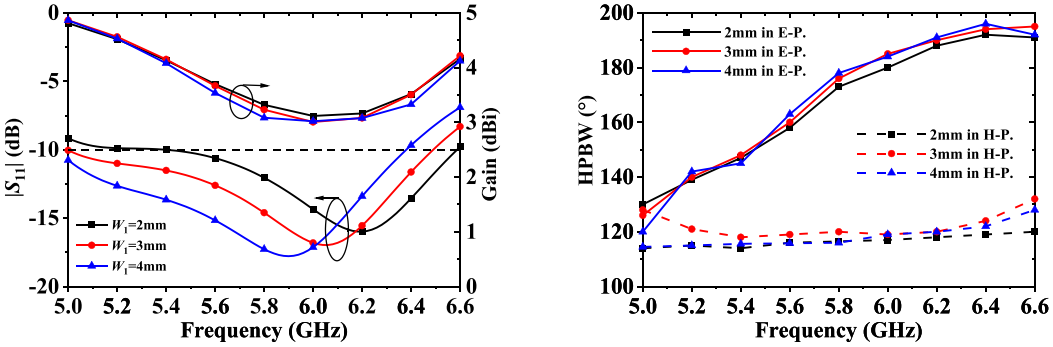

Figure 7. Simulated performances of the proposed antenna with different W_1. (a) $|S_{11}|$ and gain. (b) HPBWs in E- and H-plane.

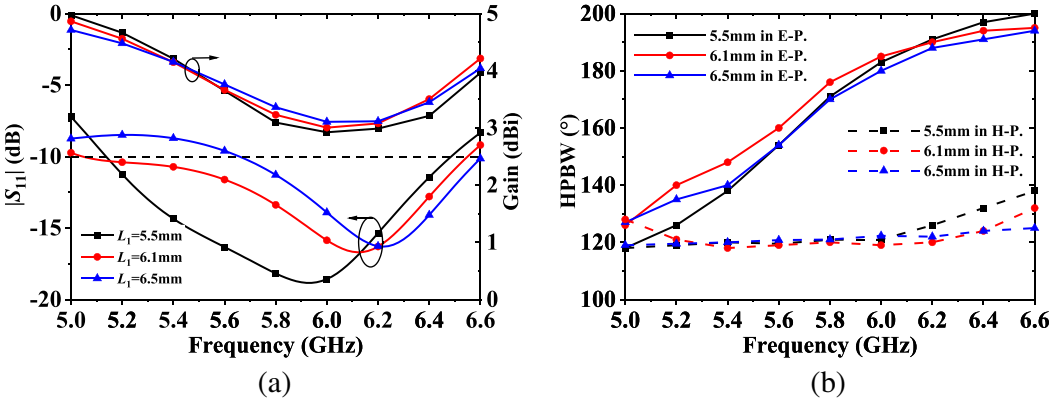

Figure 8. Simulated performances of the proposed antenna with different L_1. (a) $|S_{11}|$ and gain. (b) HPBWs in E- and H-plane.

It is noted that since the distance between the edges of the patch and substrate is fixed, and the width of the substrate, W_s, also varies with W_1. According to Fig. 6(a), it is seen that the operating bandwidth is shifted to lower frequencies when W_1 increases. However, the 10-dB FBW is nearly unchanged when W_1 varies. In detail, when W_1 is 2, 3, and 4 mm, the FBWs are 24.1%, 27.6%, and 25.9%, respectively. The reason is that as the size of the patch increases, the equivalent current length increases, which results in lowered resonant frequency. However, since the radiation performance of the patch is constant during the change of the dimension, the overall performance of the antenna is not affected by changing the variable W_1. This can be demonstrated in Fig. 7, where the in-band gain and HPBWs of the antenna are nearly unchanged. Thus, consider the 10-dB FBW and the designed center frequency of 5.8 GHz, the value of W_1 is chosen as 3 mm.

Figure 8 shows the performances of the proposed antenna with different L_1 ranging from 5.5 to 6.5 mm. It is clear that L_1 keeps a great influence on the $|S_{11}|$, especially on the lower frequencies. Besides, the impedance matching level is also influenced by L_1. When L_1 ranges from 5.5 to 6.5 mm, the 10-dB FBW is slightly increased from 23.1% to 25.5%, then decreased to 16.2%. The reason for this is similar to the variation of W_1, where L_1 and W_1 both denote the dimensions of the radiation patch. It is observed in Fig. 8(b) that the change of L_1 shows less influence on the gain and HPBW of the antenna. When L_1 equals 6.1 mm, a slightly wider E-plane HPBW and 10-dB FBW is achieved. Thus, the value of L_1 is chosen as 6.1 mm.

Figure 9 shows the performances of the proposed antenna with different L_2 ranging from 8 to 10 mm. It is seen in Fig. 9(a) that the impedance matching in the 6 to 6.4 GHz range gets better, but the in-band gain is reduced. According to Fig. 9(b), the in-band beamwidths at E-plane are narrowed

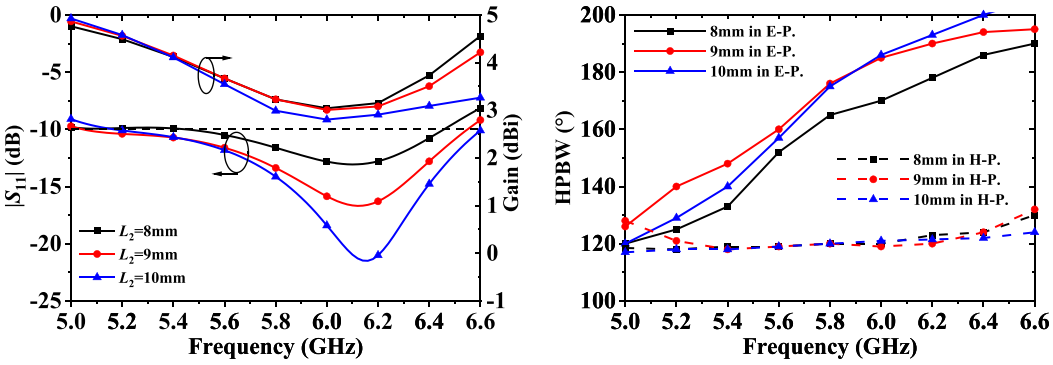

Figure 9. Simulated performances of the proposed antenna with different L_2. (a) $|S_{11}|$ and gain. (b) HPBWs in E- and H-plane.

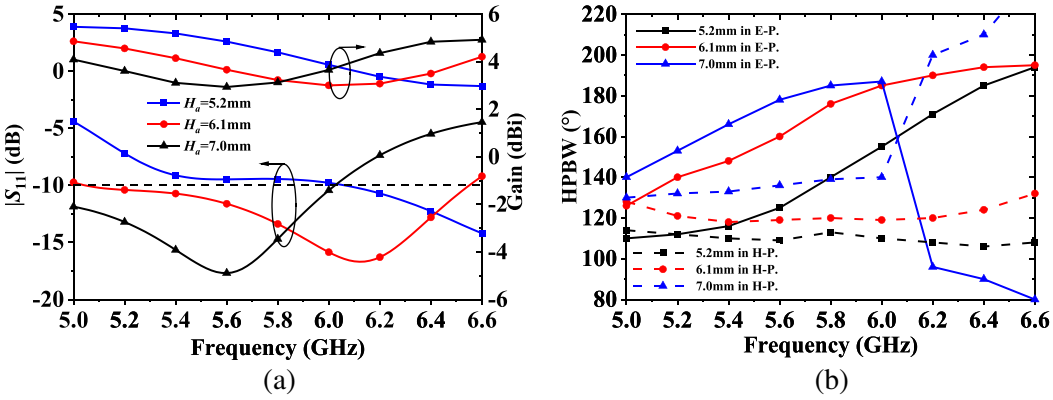

Figure 10. Simulated performances of the proposed antenna with different H_a. (a) $|S_{11}|$ and gain. (b) HPBWs in E- and H-plane.

when L_2 equals 8 mm. Compared with L_2 = 9 mm, the beamwidths in E-plane are narrower at low frequencies and wider at high frequencies when L_2 equals 10 mm. When L_2 increases, the location of the right metal column shifts more to the right side, which will influence the E-plane far-field superposition between the patch and metal column. Thus, wider HPBW at E-plane is observed. As the HPBW increases, the corresponding gain is decreased. For obtaining stable beamwidth over the operating frequency band, L_2 is chosen as 9 mm.

Figure 10 shows the performances of the proposed antenna with different H_a ranging from 5.2 to 7 mm. H_a denotes the air gap between the substrate and the ground plane, which influences both the matching and radiation performance of the antenna. In detail, the change of the air gap will vary the equivalent inductance generated by the long feeding probe, which will affect the impedance matching. Besides, it will change the length of the metal columns added on the two sides of the substrate, which results in the change of the radiation performance. It is seen from Fig. 10 that when H_a equals 5.2 or 7 mm, the operating bandwidth is overall offset to high frequency or low frequency, respectively. Besides, according to Fig. 10(b), decreasing H_a makes the in-band HPBWs smaller at E-plane, and increasing H_a will cause the radiation pattern to change at the frequencies over 6 GHz, which is manifested as the in-band gain and beamwidths at H-plane increases, and beamwidths at E-plane rapidly decrease. Considering good impedance matching over the operating band and the wide HPBW at both planes, H_a is selected as 6.1 mm.

Figure 11 shows the performances of the proposed antenna with different L_{gy} ranging from 20 to 28 mm. It is seen that the impedance matching gets better with the increase of L_{gy}, especially when $L_{gy} = 20$ mm. Besides, the HPBW at H-plane is increased as L_{gy} decreases. But the HPBW at E-plane

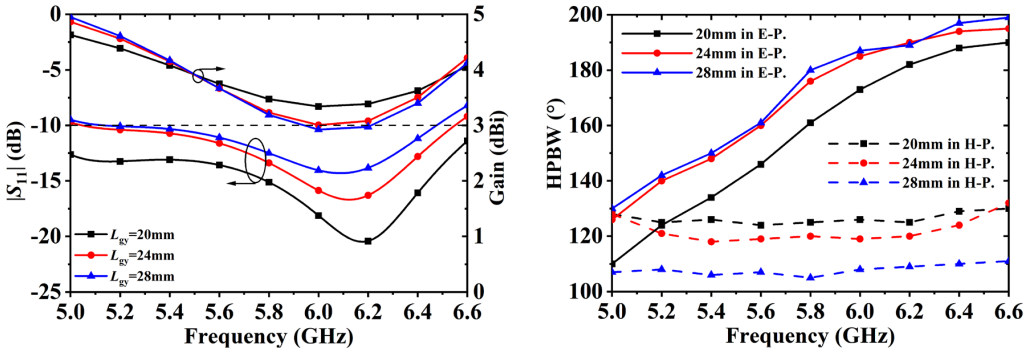

Figure 11. Simulated performances of the proposed antenna with different L_{gy}. (a) $|S_{11}|$ and gain. (b) HPBWs in E- and H-plane.

is obviously decreased as L_{gy} decreases from 24 mm to 20 mm. Thus, the dimension of the finite ground will affect the HPBW of the antenna, but has opposite influences on the E- and H-planes. According to Fig. 11(b), the in-band HPBWs at E-plane for $L_{gy} = 24$ mm are at least 10° greater than $L_{gy} = 20$ mm. When L_{gy} equals 20 or 24 mm, the difference of HPBWs at H-plane is not more than 5°. Therefore, L_{gy} is finally chosen to be 24 mm to obtain wide HPBW in both planes.

4. IMPLEMENTATION AND MEASUREMENT

To verify the proposed antenna, a prototype was fabricated and measured, where photographs are shown in Fig. 12. Table 2 shows the final optimized dimensions of the designed antenna. The measured and simulated $|S_{11}|$ and peak gains of the proposed antenna are shown in Fig. 13(a). It is observed that the simulated and measured results agree basically with slight discrepancies caused by the fabrication tolerances. Under the criterion of $|S_{11}| < -10$ dB, the simulated and measured FBWs reach 25.5% and

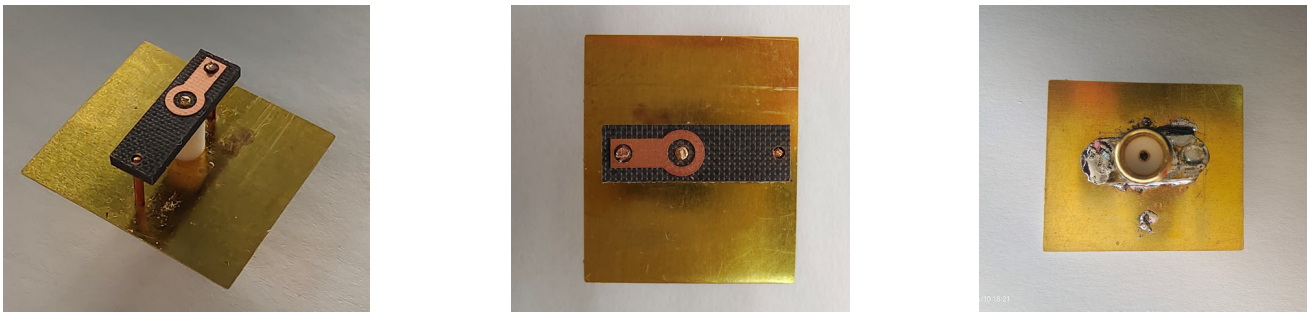

Figure 12. Photograph of the fabricated antenna. (a) 3-D view. (b) Top view. (c) Bottom view.

Table 2. Optimized dimensions of the proposed antenna.

Parameter	W_1	L_1	L_2	H_a	H_s	L_s	W_s	L_g
Units (mm)	3.5	6.1	9.0	6.1	1.5	16.4	6.0	6.9
Parameter	L_{gx}	L_{gy}	R_1	R_{g1}	R_{g2}	R_f	R_p	H_g
Units (mm)	22.4	24	1.0	2.4	1.6	1.26	4.0	0.2

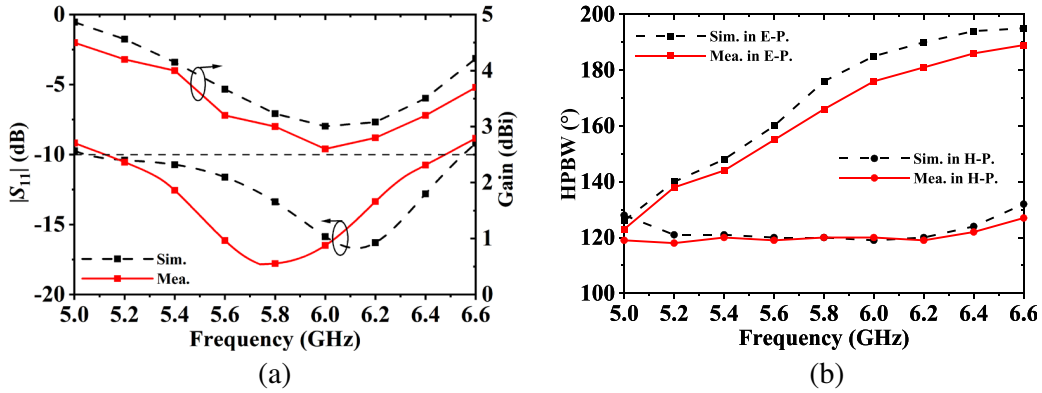

Figure 13. Simulated and measured performances of the fabricated antenna. (a) $|S_{11}|$ and gain. (b) In-band HPBW at E- and H-planes.

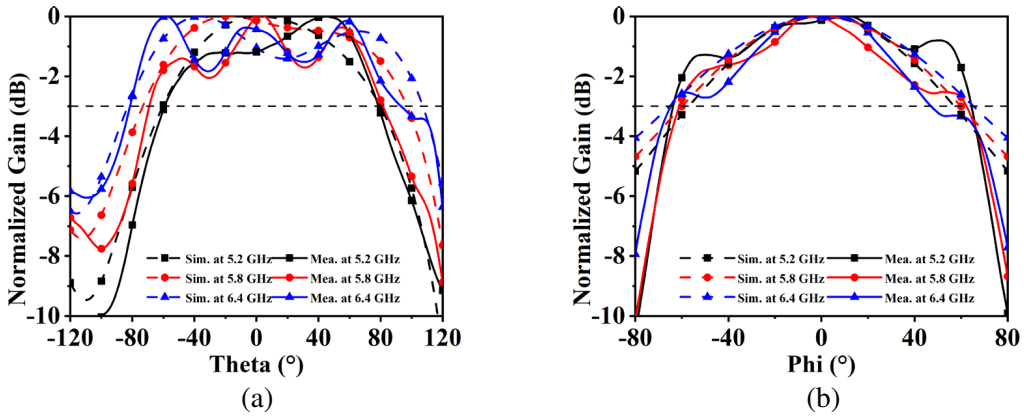

Figure 14. Simulated and measured radiation patterns of the antenna at 5.2 GHz, 5.8 GHz and 6.4 GHz. (a) E-plane. (b) H-plane.

24.1%, respectively. The in-band simulated and measured gains are in the ranges of $3 \sim 4.8$ dBi and $2.5 \sim 4.2$ dBi, respectively. A difference about 0.5 dB is observed which may be due to the fabrication error.

Figure 13(b) shows the E-plane and H-plane HPBWs versus the operating frequency. At H-plane, the simulated and measured HPBWs are kept around 120° over the bandwidth of 5.1 GHz $\sim$ 6.5 GHz. At E-plane, the simulated and measured in-band HPBWs are widened with the increase of the frequency and in the range of 130° to 190°. A difference of less than 10° is observed between the simulated and measured results. Considering the gain and HPBWs of the antenna together, it is found that from 5.1 GHz to 6 GHz, the measured gain is decreased, and the corresponding HPBW at E-plane is increased (the HPBW in H-plane is nearly constant). This trend is conformed to that the gain decreases as HPBW increases. In this bandwidth, the change of the HPBW is obviously from 120° to 175°. Thus, an obvious gain reduction is found from 4.8 dBi to 3 dBi. When the frequency is higher than 6 GHz, the trend is reversed. This may be because the gain is increased as the frequency increases. However, in this bandwidth, the variation of the HPBW at E-plane is not obvious (from 175° to 190°). Thus, the increase of HPBW cannot decrease the gain obviously. Besides, the measured gains and HPBWs are both lower than the simulated ones. This may be due to the measurement errors. In the anechoic chamber, the measurement error of the gain is about 1 dB. Since the fabricated antenna is small, the feeding line which connects the antenna to the rotary table will influence the radiation of the antenna, resulting in reduced measured HPBW. For clear description, the simulated and measured radiation patterns at 5.2 GHz, 5.8 GHz, and 6.4 GHz are plotted in Fig. 14. It is observed that at the E- and

H-planes, the measured radiation patterns are similar to the simulated ones. Stable and symmetrical radiations are obtained over the operating bandwidth.

Table 3 compares the performances of the proposed antenna with that of various representative wide-beam antennas. Compared with the antennas in [6] and [7], the proposed design shows wider bandwidth. In comparison with the antennas in [8, 13], the HPBW of the proposed antenna is wider. For the antennas in [7, 8, 17], despite having an enough impedance matching bandwidth, only the HPBW of the center frequency is described. Although [15] and [16] keep sufficient impedance matching bandwidths and HPBWs, they have relatively large dimensions and complex structures, such as curved feeder probes and irregular metal arms, which causes the performance of the antenna to be greatly affected by processing errors. The main advantage of the proposed design is the small size. It is observed that the dimension of the designed antenna is the smallest among the antennas in the comparison table. At the same time, the proposed antenna also maintains wide bandwidth and beam.

Table 3. Performances comparison between the proposed and representative wide-beam antennas.

Ref.	type	freq. (GHz)	10-dB FBW (%)	HPBW (°)		Size ($\lambda_0 \times \lambda_0 \times \lambda_0$)[a]
				E-plane	H-plane	
[6]	Microstrip	5.9	13	90–150	100–111	$0.33 \times 0.33 \times 0.03$
[7]	Microstrip	4	15	221[b]	168[b]	$0.43 \times 0.35 \times 0.3$
[8]	Microstrip	3.5	40	174[b]	112[b]	$0.35 \times 0.35 \times 0.21$
[13]	Dipole	31	47.5	120[c]	120[c]	$0.44 \times 0.27 \times 0.18$
[15]	Dipole	5.5	81	106–217	83–186	$0.43 \times 0.37 \times 0.16$
[16]	Dipole	1.9	94.9	103–146	110–179	$0.43 \times 0.58 \times 0.25$
[17]	Dipole	9	33	156[b]	360[b]	$0.45 \times 0.27 \times 0.1$
This work	Microstrip	5.8	24.1	130–190	118–124	$0.31 \times 0.11 \times 0.11$

[a] λ_o is the waveguide wavelength at the center frequency.

[b] Value at the center frequency.

[c] The minimum value within the operating band.

5. CONCLUSION

In this paper, a compact antenna is proposed, which exhibits the merits of small size, compact structure, wideband, and wide HPBW. By loading two metal columns on both sides of the radiation element, the HPBW at E-plane is obviously widened with symmetrical radiation patterns and miniaturized size. Measurement shows that the dimension of the fabricated radiation element is only $0.31\lambda_0 \times 0.11\lambda_0 \times 0.11\lambda_0$. Under the criterion of more than 10 dB return loss, the measured FBW is 24.2%. In the bandwidth, the HPBW at E-plane is in the range of $130^\circ \sim 190^\circ$, and the values are around 120° at H-plane. Because the proposed antenna shows wideband and wide beam with compact structure, it can be a candidate for high integration wideband wide-angle scanning applications.

ACKNOWLEDGMENT

This work was supported in part by the National Natural Science Foundation of China under Grant 51809030, in part by the Liaoning Revitalization Talents Program under Grant XLYC2007067, in part by the Young Elite Scientists Sponsorship Program by CAST under Grant 2022QNRC001 and in part by the Fundamental Research Funds for the Central Universities under Grant 3132023246.

REFERENCES

1. Valavan, S. E., D. Tran, A. G. Yarovoy, and A. G. Roederer, "Dual-band wide-angle scanning planar phased array in/Ku-bands," *IEEE Trans. Antennas Propag.*, Vol. 62, No. 5, 2514–2521, May 2014.
2. Yang, G., J. Li, R. Xu, Y. Ma, and Y. Qi, "Improving the performance of wide-angle scanning array antenna with a high-impedance periodic structure," *IEEE Antennas Wireless Propag. Lett.*, Vol. 15, 1819–1822, 2016.
3. Beenamole, K. S., P. N. S. Kutiyal, U. K. Revankar, and V. M. Pandharipande, "Resonant microstrip meander line antenna element for wide scan angle active phased array antennas," *Microw. Opt. Technol. Lett.*, Vol. 50, No. 7, 1737–1740, 2008.
4. Chen, X., P.-Y. Qin, Y. J. Guo, and G. Fu, "Low-profile and wide-beamwidth dual-polarized distributed microstrip antenna," *IEEE Access*, Vol. 5, 2272–2280, 2017.
5. Liu, C.-M., S. Xiao, and X.-L. Zhang, "A compact, low-profile wire antenna applied to wide-angle scanning phased array," *IEEE Antennas Wireless Propag. Lett.*, Vol. 17, No. 3, 389–392, Mar. 2018.
6. Feng, Y., et al., "A broadband wide-angle scanning linear array antenna with suppressed mutual coupling for 5G sub-6G applications," *IEEE Antennas Wireless Propag. Lett.*, Vol. 21, No. 2, 366–370, Feb. 2022.
7. Yang, G., J. Li, S. G. Zhou, and Y. Qi, "A wide-angle E-plane scanning linear array antenna with wide beam elements," *IEEE Antennas Wireless Propag. Lett.*, Vol. 16, 2923–2926, 2017.
8. Yang, G., J. Li, D. Wei, and R. Xu, "Study on wide-angle scanning linear phased array antenna," *IEEE Trans. Antennas and Propag.*, Vol. 66, No. 1, 450–455, Jan. 2018.
9. Yang, G., Y. Zhang, and S. Zhang, "Wide-band and wide-angle scanning phased array antenna for mobile communication system," *IEEE Open Journal of Antennas and Propagation*, Vol. 2, 203–212, 2021.
10. Zeng, J. and K.-M. Luk, "A simple wideband magnetoelectric dipole antenna with a defected ground structure," *IEEE Antennas Wireless Propag. Lett.*, Vol. 17, No. 8, 1497–1500, Aug. 2018.
11. Li, M. and K.-M. Luk, "Wideband magneto-electric dipole antenna for 60-GHz millimeter-wave communications," *IEEE Trans. Antennas Propag.*, Vol. 63, No. 7, 3276–3279, Jul. 2015.
12. Qiu, W., C. Chen, and W. Chen, "A broadband magnetoelectric dipole antenna with stable wide beamwidth," *2016 IEEE International Symposium on Antennas and Propagation (APSURSI)*, 1849–1850, Fajardo, PR, USA, 2016.
13. Xiao, Z., Y. Pan, X. Liu, and K. W. Leung, "A wideband magnetoelectric dipole antenna with wide beamwidth for millimeter-wave applications," *IEEE Antennas Wireless Propag. Lett.*, Vol. 22, No. 4, 918–922, Apr. 2023.
14. Chang, L., L.-L. Chen, J.-Q. Zhang, and Z.-Z. Chen, "A compact wideband dipole antenna with wide beamwidth," *IEEE Antennas Wireless Propag. Lett.*, Vol. 20, No. 9, 1701–1705, Sept. 2021.
15. Kim, Y.-B., H.-J. Dong, K.-S. Kim, and H. L. Lee, "Compact planar multipole antenna for scalable wide beamwidth and bandwidth characteristics," *IEEE Trans. Antennas and Propag.*, Vol. 68, No. 5, 3433–3442, May 2020.
16. Yang, G., J. Li, J. Yang and S.-G. Zhou, "A wide beamwidth and wideband magnetoelectric dipole antenna," *IEEE Trans. Antennas Propag.*, Vol. 66, No. 12, 6724–6733, Dec. 2018.
17. Yang, H., X. Cao, J. Gao, H. Yang, and T. Li, "A wide-beam antenna for wide-angle scanning linear phased arrays," *IEEE Antennas Wireless Propag. Lett.*, Vol. 19, No. 12, 2122–2126, Dec. 2020.
18. Wang, Z., S. Zhao, and Y. Dong, "Metamaterial-based wide-beam dielectric resonator antenna for broadband wide-angle beam-scanning phased array applications," *IEEE Trans. Antennas Propag.*, Vol. 70, No. 10, 9061–9072, Oct. 2022.
19. Li, R.-Y., Y.-C. Jiao, Y.-X. Zhang, L. Zhang, and H.-Y. Wang, "A DRA with engraved groove and comb-like metal wall for beamwidth enhancement in both E- and H-planes," *IEEE Antennas Wireless Propag. Lett.*, Vol. 20, No. 4, 543–547, Apr. 2021.